SUPPORTING INFORMATION

High brightness and easy color modulation in lanthanide-based coordination polymers with 5-methoxyisophthalate as ligand: Toward emission colors additive strategy

Insa Badiane[a,b], Stéphane Freslon[a], Yan Suffren[a], Carole Daiguebonne[a]*, Guillaume Calvez[a], Kevin Bernot[a], Magatte Camara[b] and Olivier Guillou[a]*.

[a] INSA Rennes, UMR 6226 "Institut des Sciences Chimiques de Rennes", 20 Avenue des buttes de Coësmes, F35708 Rennes

[b] Université Assane Seck de Ziguinchor, LCPM – Groupe "Matériaux Inorganiques: Chimie Douce et Cristallographie". BP. 523 Ziguinchor – Sénégal

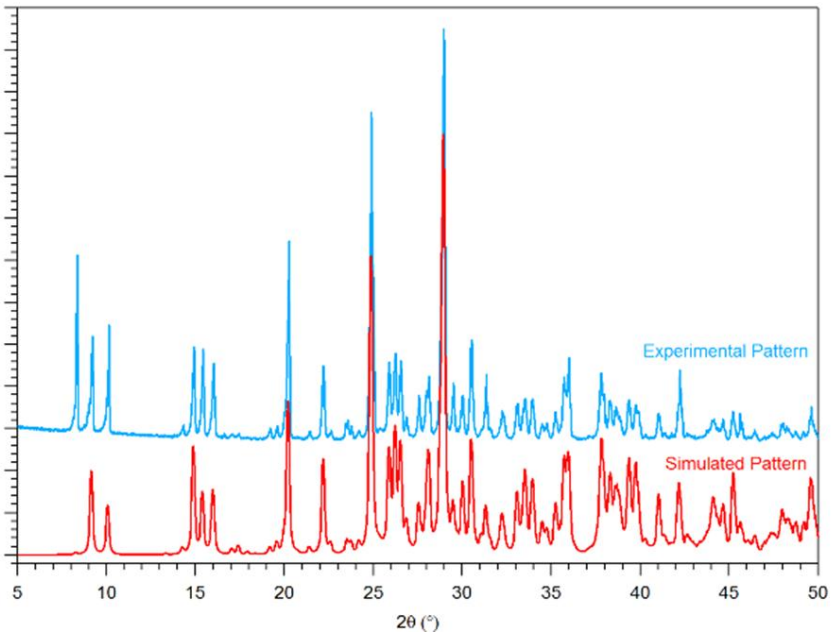

Figure S1. Experimental and simulated (on the basis of the crystal structure) powder X-ray diffraction patterns of $Na_2(mip)\cdot 7H_2O$.

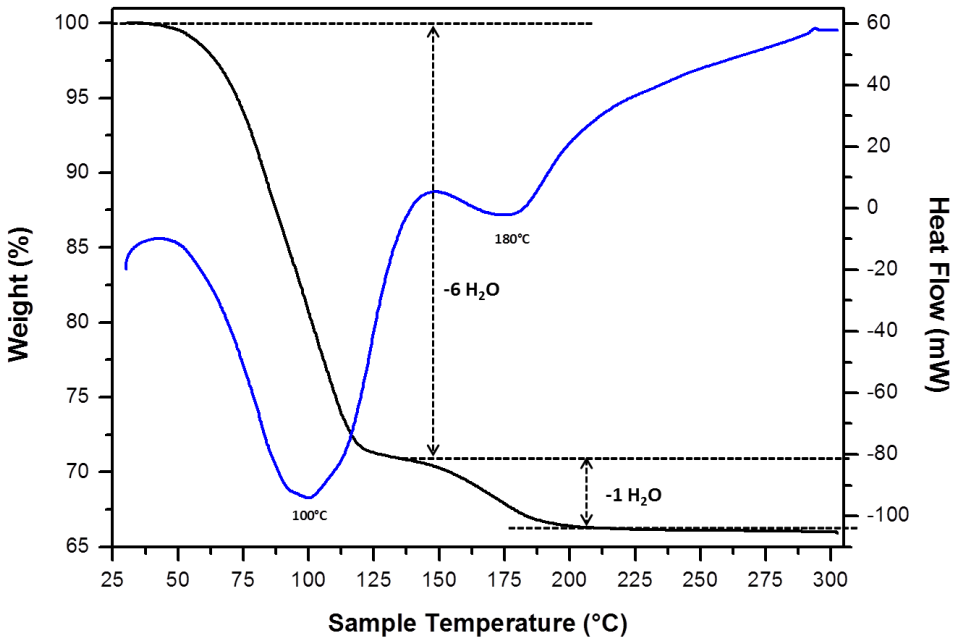

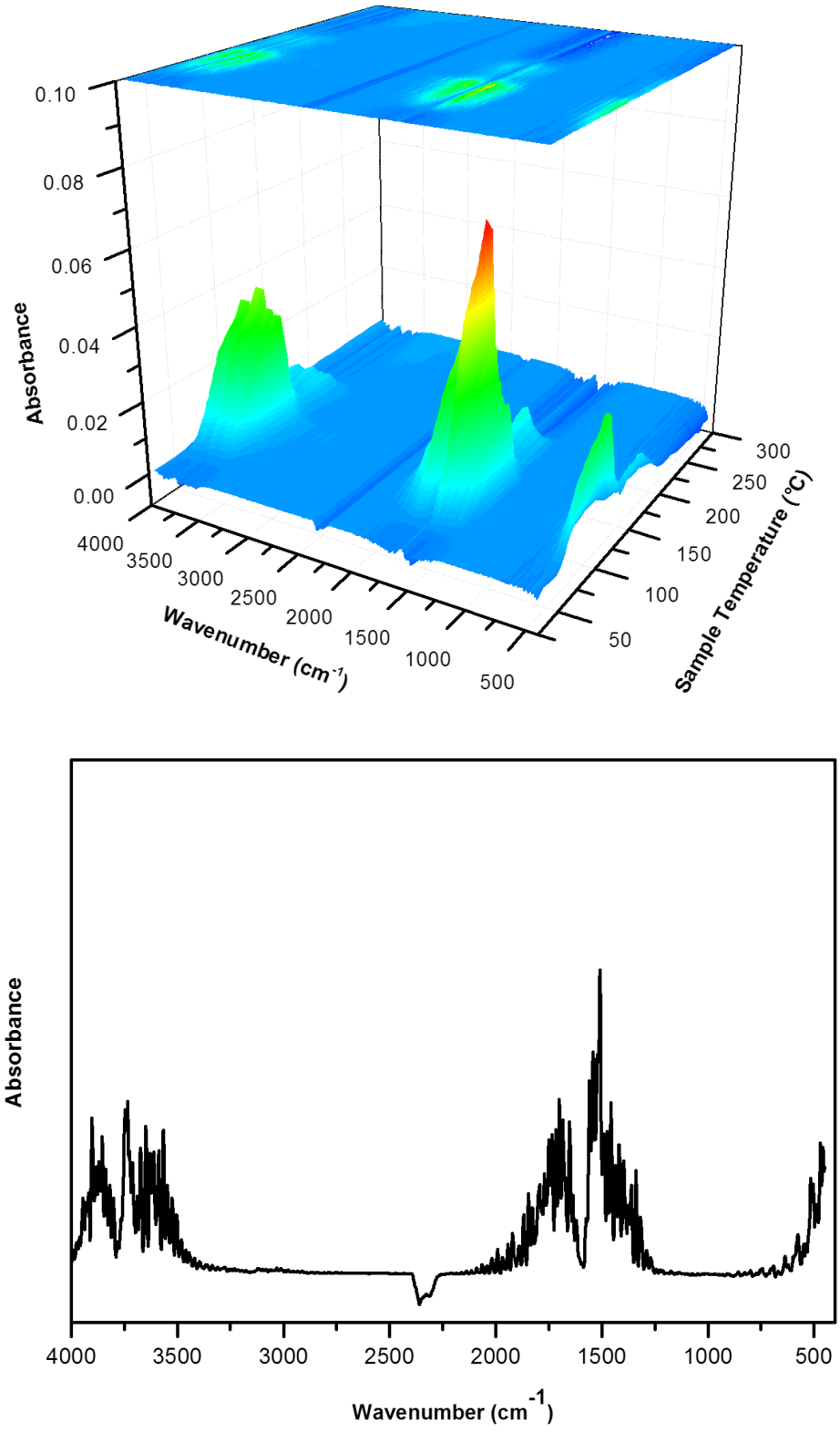

Figure S2. Top: ATG/DSC of $Na_2(mip)\cdot 7H_2O$ between room temperature and 300°C under N_2 flux. Middle: IR spectra of the exhausted gas during thermal analyses versus temperature. Bottom: IR spectrum recorded at T=90°C.

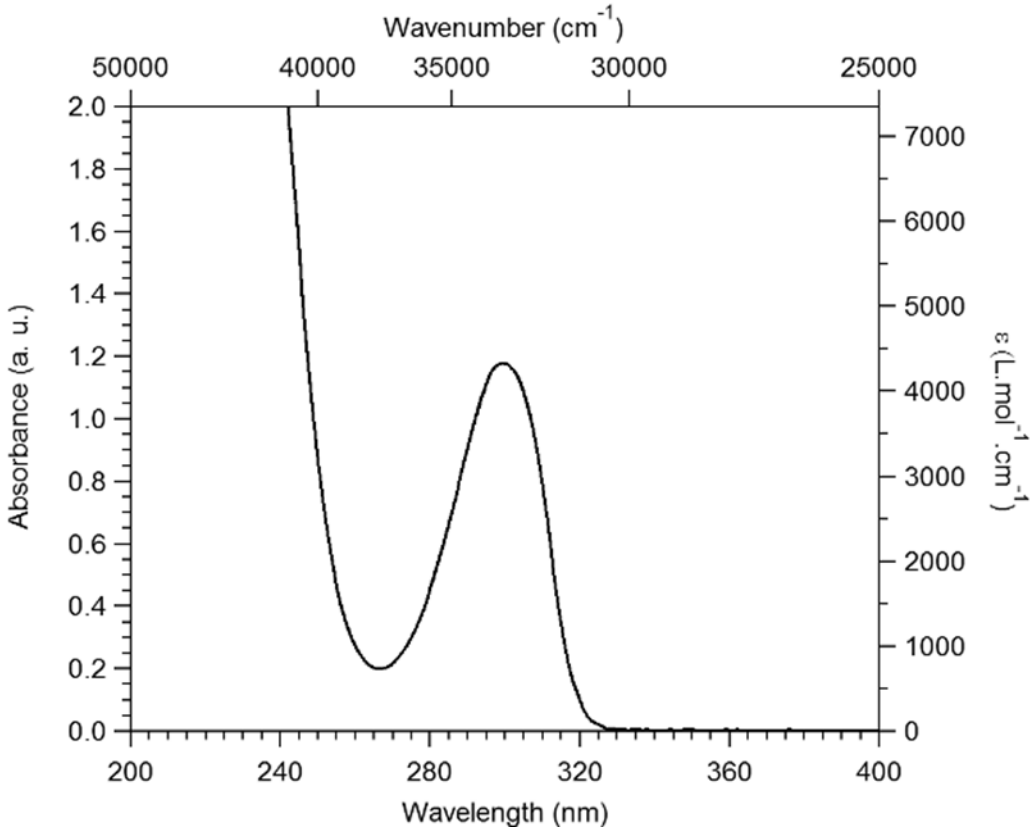

Figure S3. Liquid state UV-visible absorption spectrum of a diluted ($2.73\ 10^{-4}$ mol.L^{-1}) aqueous solution of $Na_2(mip)\cdot 7H_2O$

Table S1. Chemical analyzes for compounds that constitute families **(1)** and **(2)**.

Chemical formula	MW (g.mol^{-1})	%C calc. (found)	%H calc. (found)	%O calc. (found)	%Ln calc. (found)
$[La(mip)(Hmip)(H_2O)_5\cdot H_2O]_\infty$	635.9	34.0 (34.2)	3.9 (4.1)	40.3 (40.1)	21.8 (21.6)
$[Ce(mip)(Hmip)(H_2O)_5\cdot H_2O]_\infty$	637.1	33.9 (33.9)	3.9 (3.8)	40.2 (40.3)	22.0 (22.0)
$[Sm_2(mip)_3(H_2O)_8\cdot 4H_2O]_\infty$	1098.8	29.5 (29.4)	3.8 (3.6)	39.3 (39.5)	27.4 (27.5)
$[Eu_2(mip)_3(H_2O)_8\cdot 4H_2O]_\infty$	1102.0	29.4 (29.6)	3.8 (3.4)	39.2 (39.4)	27.6 (27.6)
$[Gd_2(mip)_3(H_2O)_8\cdot 4H_2O]_\infty$	1112.6	29.1 (29.4)	3.8 (3.5)	38.8 (38.4)	28.3 (28.7)
$[Tb_2(mip)_3(H_2O)_8\cdot 4H_2O]_\infty$	1115.8	29.0 (29.1)	3.8 (3.5)	38.7 (38.4)	28.5 (29.0)
$[Dy_2(mip)_3(H_2O)_8\cdot 4H_2O]_\infty$	1123.0	28.9 (28.9)	3.7 (3.3)	38.5 (39.0)	28.9 (28.8)
$[Ho_2(mip)_3(H_2O)_8\cdot 4H_2O]_\infty$	1127.8	28.7 (28.9)	3.7 (3.4)	38.3 (38.3)	29.2 (29.4)
$[Er_2(mip)_3(H_2O)_8\cdot 4H_2O]_\infty$	1132.6	28.6 (28.5)	3.7 (3.4)	38.1 (38.2)	29.5 (29.9)
$[Y_2(mip)_3(H_2O)_8\cdot 4H_2O]_\infty$	975.8	33.2 (33.1)	4.3 (4.4)	44.3 (44.2)	18.2 (18.3)

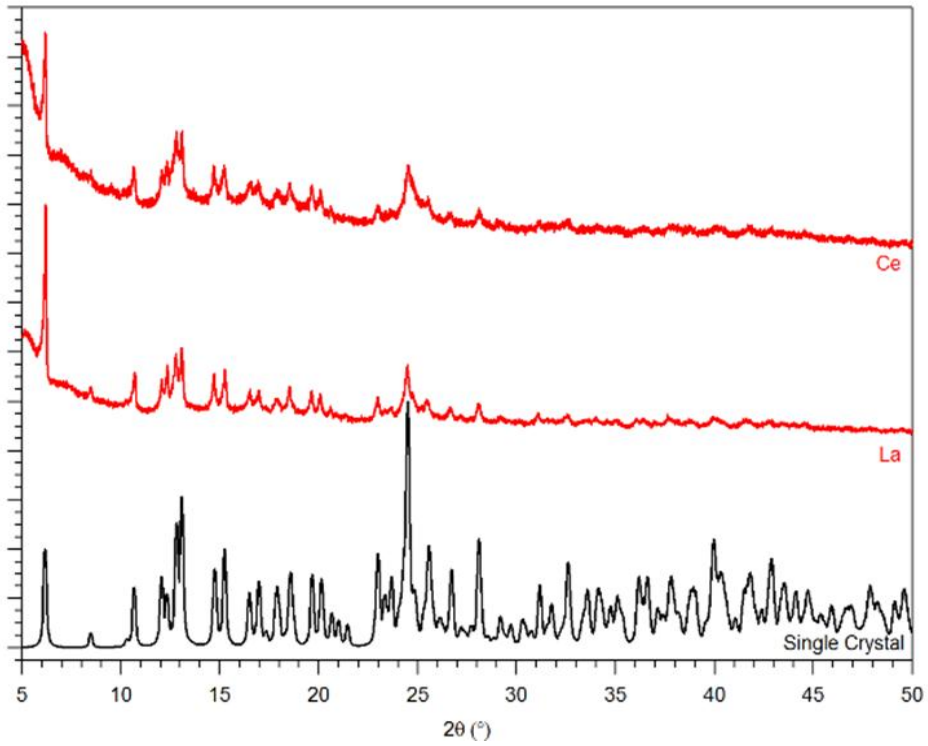

Figure S4. Experimental and simulated powder X-ray diffraction patterns of compounds with general chemical formula $[Ln(mip)(Hmip)(H_2O)_5 \cdot H_2O]_\infty$ with Ln = La or Ce. Simulated diagram has been drawn on the basis of the corresponding crystal structure.

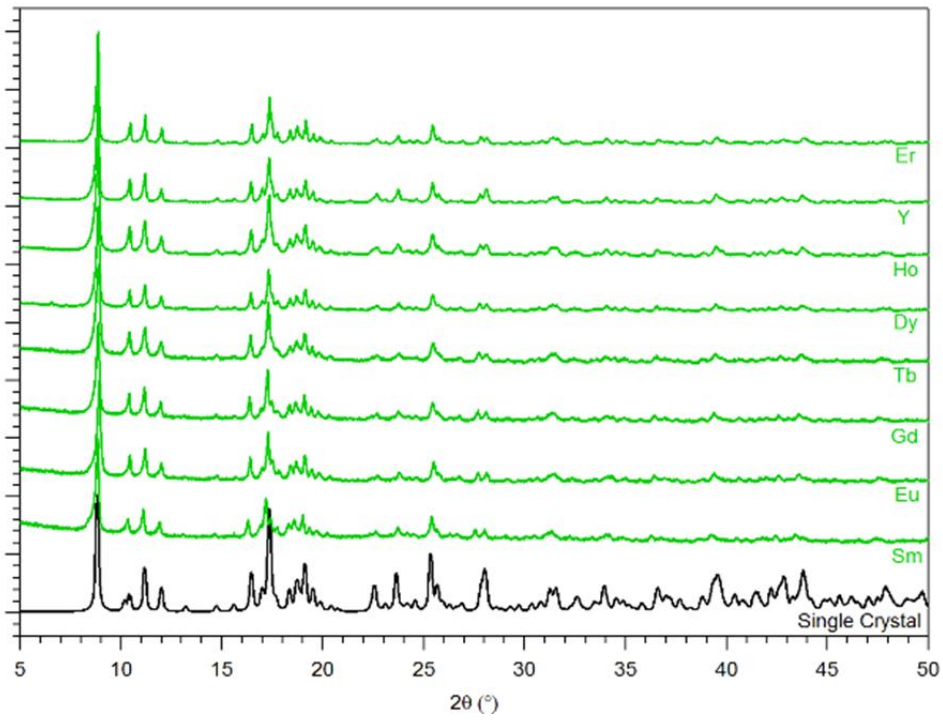

Figure S5. Experimental and simulated powder X-ray diffraction patterns of compounds that have general chemical formula $[Ln_2(mip)_3(H_2O)_8 \cdot 4H_2O]_\infty$ with Ln = Sm-Er plus Y. Simulated diagram has been drawn on the basis of the corresponding crystal structure.

Table S2. Continuous Shape Measurements (CSM) performed on the Ce center of $[Ce(mip)_{3/2}(H_2O)_5 \cdot 2H_2O]_\infty$.

Atom label	Ce1
Lowest CSM value	1.709
Associated polyhedron, site symmetry	Muffin, *Cs*
2nd lowest CSM value	2.605
Associated polyhedron, site symmetry	Capped square antiprism, *C4v*
3rd lowest CSM value	2.765
Associated polyhedron, site symmetry	Tricapped trigonal prism, *D3h*

Lowest values indicates best agreement to theoretical coordination polyhedra symmetry (whose CSM = 0.000).

Table S3. Continuous Shape Measurements (CSM) performed on the Gd center of $[Gd(mip)(Hmip)(H_2O)_5 \cdot H_2O]_\infty$.

Atom label	Gd
Lowest CSM value	0.644
Associated polyhedron, site symmetry	Capped square antiprism, *C4v*
2nd lowest CSM value	1.134
Associated polyhedron, site symmetry	Muffin, *Cs*
3rd lowest CSM value	1.604
Associated polyhedron, site symmetry	Tricapped trigonal prism, *D3h*

Lowest values indicates best agreement to theoretical coordination polyhedra symmetry (whose CSM = 0.000).

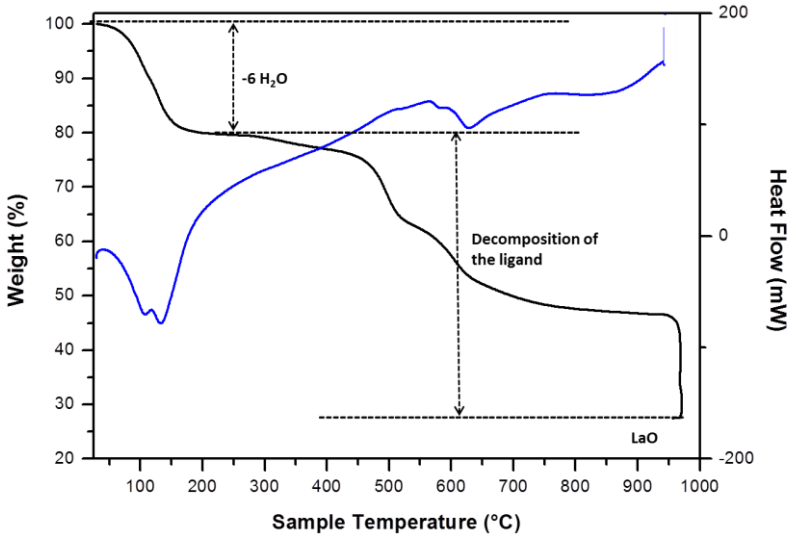

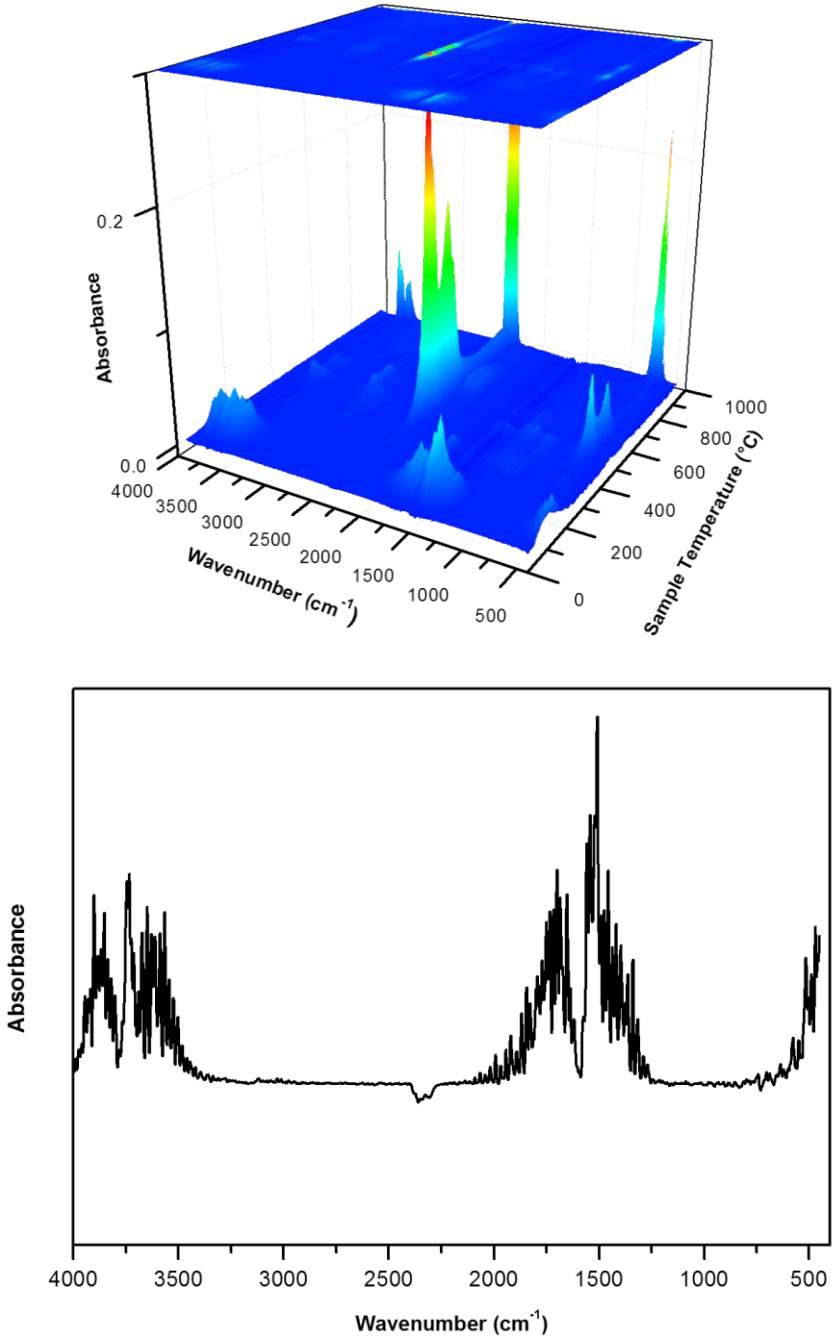

Figure S6. Top: ATG/DSC of $[La(mip)(Hmip)(H_2O)_5].H_2O]_\infty$. Middle: IR spectra versus temperature of the exhausted gas during thermal analysis. Bottom: IR spectrum recorded at 90°C.

Table S4. Continuous Shape Measurements (CSM) performed on the Y centers of $[Ln_2(mip)_3(H_2O)_8 \cdot 4H_2O]_\infty$

Atom label	Y1	Y2
Lowest CSM value	2.099	2.034
Associated polyhedron, site symmetry	Capped square antiprism, *C*4*v*	Capped square antiprism, *C*4*v*
2nd lowest CSM value	2.130	2.042
Associated polyhedron, site symmetry	Muffin, *Cs*	Muffin, *Cs*
3rd lowest CSM value	2.815	2.675
Associated polyhedron, site symmetry	Tricapped trigonal prism, *D*3*h*	Tricapped trigonal prism, *D*3*h*

Lowest values indicates best agreement to theoretical coordination polyhedra symmetry (whose CSM = 0.000).

Table S5. Selected hydrogen-bond distances in $[Y_2(mip)_3(H_2O)_8 \cdot 4H_2O]_\infty$.

Atom 1	Atom2	Symmetry	Distance (Å)
O027	O032	2-x, 1-y, 1-z	2.7077(2)
O006	O015	x, y, z	2.7519(1)
O005	O015	x, y, z	2.7683(1)
O007	O026	2-x, 1-y, 1-z	2.7930(2)
O007	O011	x, y, z	2.8049(1)
O023	O032	2.5-x, -0.5+y, 1.5-z	2.8355(1)
O006	O018	x, y, z	2.8877(2)
O007	O021	x, y, z	2.9090(2)
O027	O027	2-x, 1-y, 1-z	2.9118(2)
O021	O028	2.5-x, -0.5+y, 1.5-z	3.0292(2)
O015	O032	2.5-x, -0.5+y, 0.5-z	3.4510(2)
O023	O028	2.5-x, -0.5+y, 1.5-z	3.5923(2)

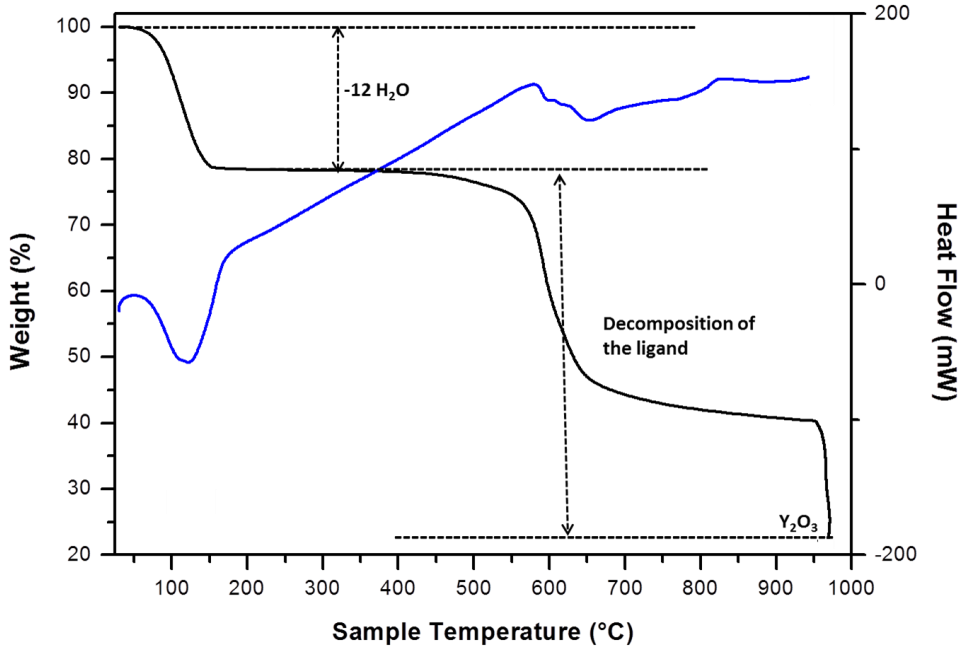

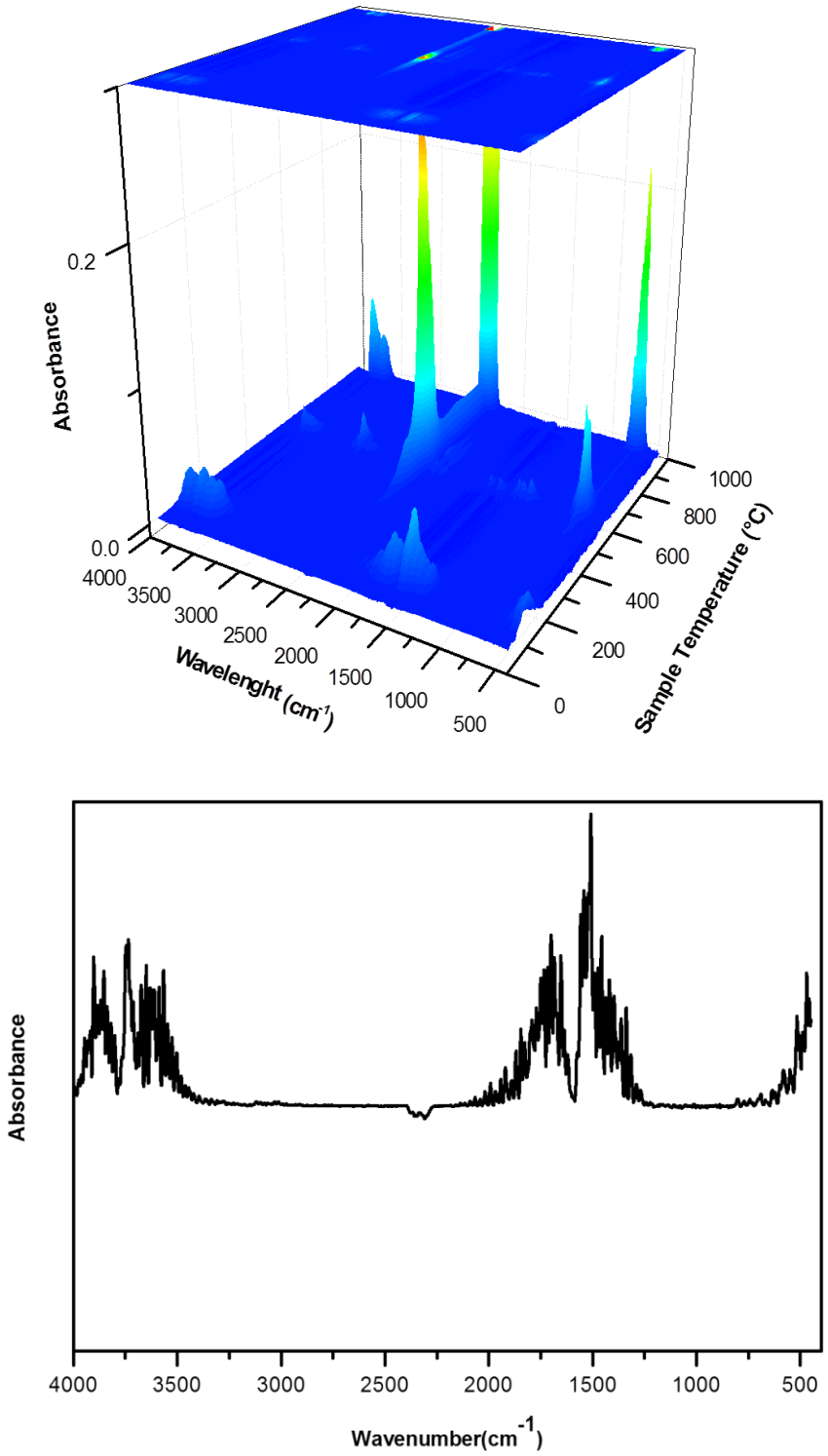

Figure S7. Top: ATG/DSC of $[Y_2(mip)_3(H_2O)_8 \cdot 4H_2O]_\infty$. Middle: IR spectra versus temperature of the exhausted gas during thermal analysis. Bottom: IR spectrum recorded at 90°C.

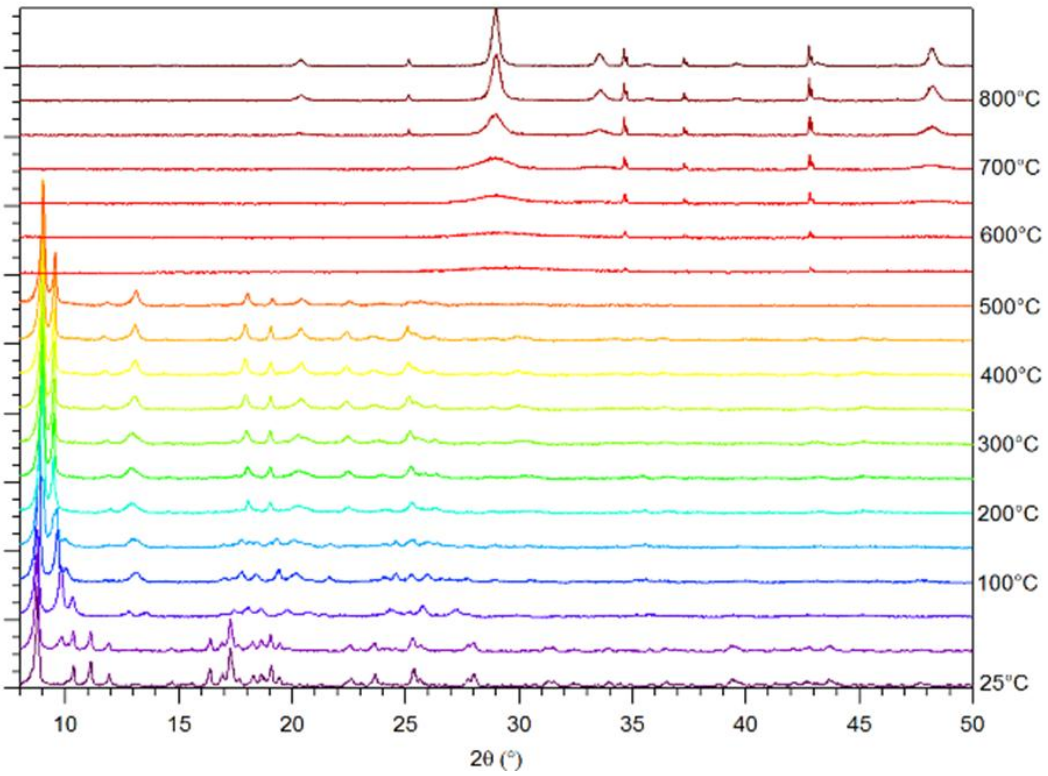

Figure S8. Thermo-dependent powder X-ray diffraction patterns of $[Y_2(mip)_3(H_2O)_8{\cdot}4H_2O]_\infty$.

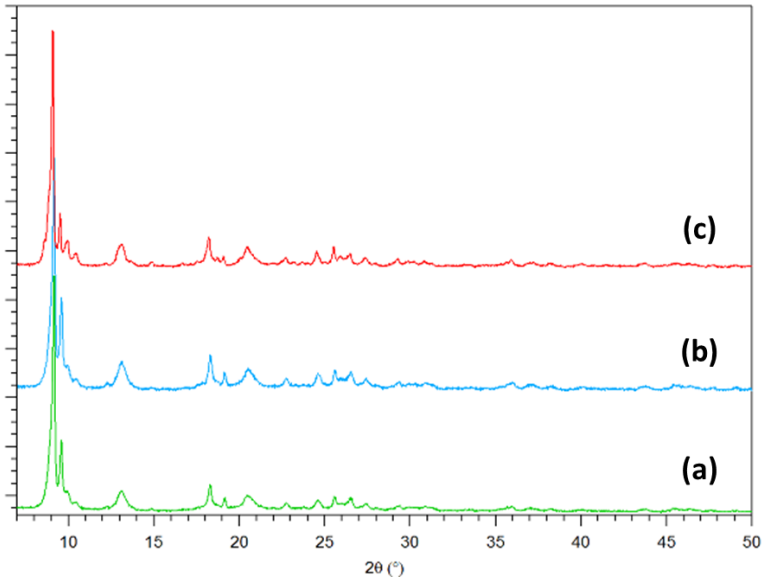

Figure S9. Powder X-ray diffraction patterns of $[Y_2(mip)_3]_\infty$: **(a)** as obtained by dehydration at 200°C ; **(b)** after exposure to ambient air ; **(c)** after immersion in water.

Table S6. Numerical values for colorimetric coordinates and luminance of $Na_2(mip)\cdot 7H_2O$ and $[Ln_2(mip)_3(H_2O)_8\cdot 4H_2O]_\infty$ with Ln = Sm-Dy under UV excitation (λ_{exc} = 312 nm).			
	Colorimetric coordinates		Luminance
	x	y	($Cd.m^{-2}$)
$Na_2(mip)\cdot 7H_2O$	0.200(5)	0.144(5)	-
$[Sm_2(mip)_3(H_2O)_8\cdot 4H_2O]_\infty$	0.430(5)	0.264(5)	0.35(5)
$[Eu_2(mip)_3(H_2O)_8\cdot 4H_2O]_\infty$	0.681(5)	0.319(5)	3.3(1)
$[Gd_2(mip)_3(H_2O)_8\cdot 4H_2O]_\infty$	0.221(5)	0.140(5)	0.62(5)
$[Tb_2(mip)_3(H_2O)_8\cdot 4H_2O]_\infty$	0.321(5)	0.616(5)	107(5)
$[Dy_2(mip)_3(H_2O)_8\cdot 4H_2O]_\infty$	0.371(5)	0.387(5)	1.7(2)

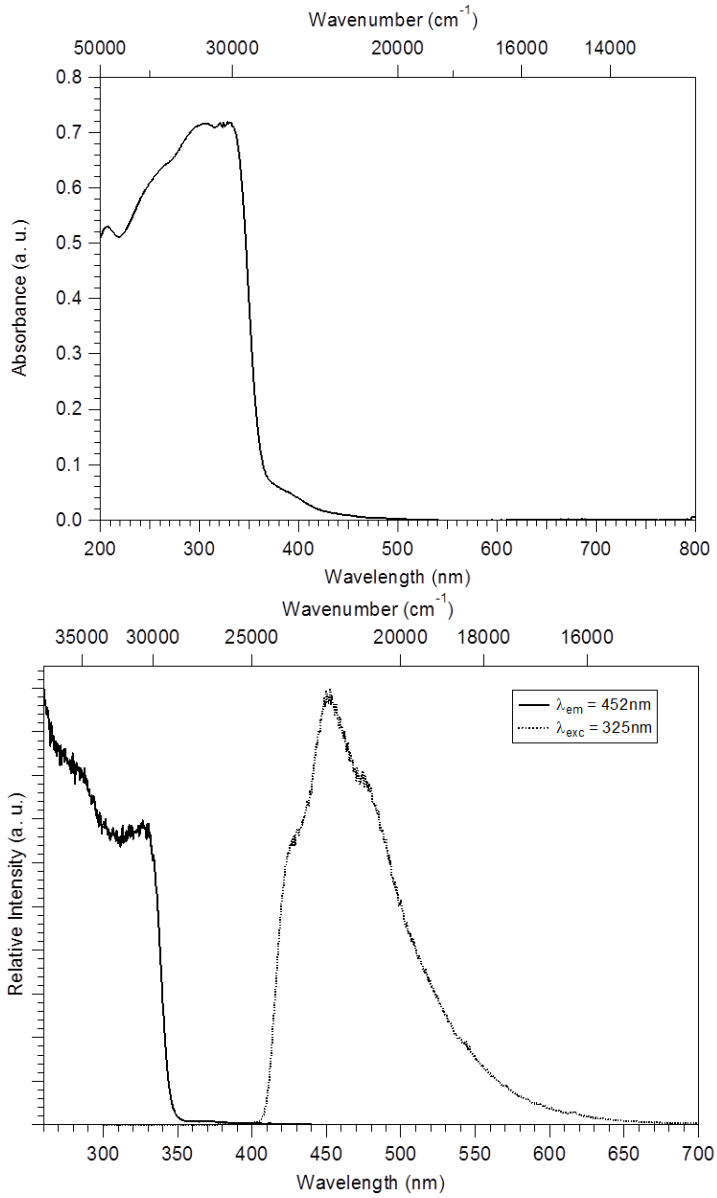

Figure S10. Top: Solid state UV-vis absorption spectrum of $[Gd_2(mip)_3(H_2O)_8\cdot 4H_2O]_\infty$. Bottom: Solid state excitation and emission spectra recorded at 77K of $[Gd_2(mip)_3(H_2O)_8\cdot 4H_2O]_\infty$.

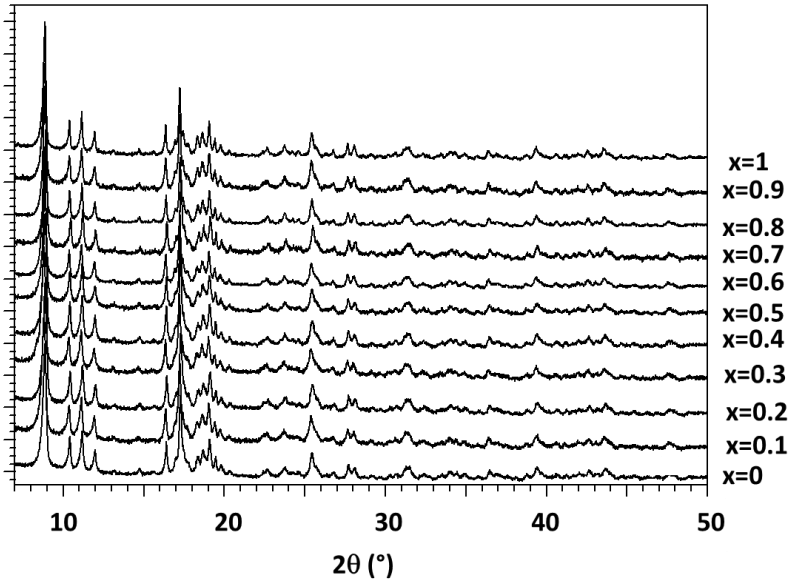

Figure S11. Powder diffraction diagrams of $[Tb_{2-2x}Gd_{2x}(mip)_3(H_2O)_8 \cdot 4H_2O]_\infty$ with $0 \leq x \leq 1$.

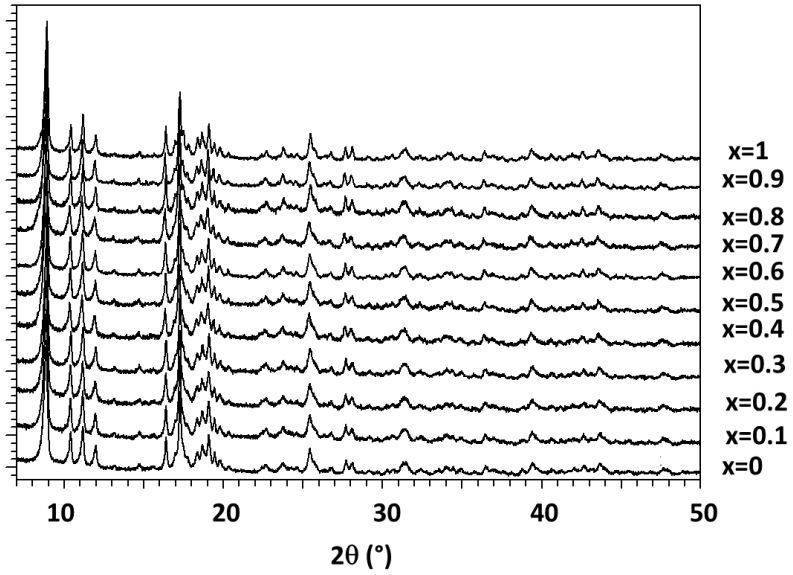

Figure S12. Powder diffraction diagrams of $[Tb_{2-2x}Eu_{2x}(mip)_3(H_2O)_8 \cdot 4H_2O]_\infty$ with $0 \leq x \leq 1$.

Table S7. Metallic contents measured by EDS for $[Tb_{2-2x}Gd_{2x}(mip)_3(H_2O)_8{\cdot}4H_2O]_\infty$ with $0 < x < 1$

	Expected ratios		Measured ratios	
	%Gd	%Tb	%Gd	%Tb
$[Tb_{1.8}Gd_{0.2}(mip)_3(H_2O)_8{\cdot}4H_2O]_\infty$	10	90	12(1)	88(1)
$[Tb_{1.6}Gd_{0.4}(mip)_3(H_2O)_8{\cdot}4H_2O]_\infty$	20	80	23(1)	77(1)
$[Tb_{1.4}Gd_{0.6}(mip)_3(H_2O)_8{\cdot}4H_2O]_\infty$	30	70	34(1)	66(1)
$[Tb_{1.2}Gd_{0.8}(mip)_3(H_2O)_8{\cdot}4H_2O]_\infty$	40	60	43(1)	57(1)
$[Tb_{1.0}Gd_{1.0}(mip)_3(H_2O)_8{\cdot}4H_2O]_\infty$	50	50	55(1)	45(1)
$[Tb_{0.8}Gd_{1.2}(mip)_3(H_2O)_8{\cdot}4H_2O]_\infty$	60	40	65(1)	35(1)
$[Tb_{0.6}Gd_{1.4}(mip)_3(H_2O)_8{\cdot}4H_2O]_\infty$	70	30	73(1)	27(1)
$[Tb_{0.4}Gd_{1.6}(mip)_3(H_2O)_8{\cdot}4H_2O]_\infty$	80	20	82(1)	18(1)
$[Tb_{0.2}Gd_{1.8}(mip)_3(H_2O)_8{\cdot}4H_2O]_\infty$	90	10	93(1)	7(1)

Table S8. Metallic contents measured by EDS for $[Tb_{2-2x}Eu_{2x}(mip)_3(H_2O)_8{\cdot}4H_2O]_\infty$ with $0 < x < 1$

	Expected ratios		Measured ratios	
	%Eu	%Tb	%Eu	%Tb
$[Tb_{1.8}Eu_{0.2}(mip)_3(H_2O)_8{\cdot}4H_2O]_\infty$	10	90	10(1)	90(1)
$[Tb_{1.6}Eu_{0.4}(mip)_3(H_2O)_8{\cdot}4H_2O]_\infty$	20	80	22(1)	78(1)
$[Tb_{1.4}Eu_{0.6}(mip)_3(H_2O)_8{\cdot}4H_2O]_\infty$	30	70	33(1)	67(1)
$[Tb_{1.2}Eu_{0.8}(mip)_3(H_2O)_8{\cdot}4H_2O]_\infty$	40	60	44(1)	56(1)
$[Tb_{1.0}Eu_{1.0}(mip)_3(H_2O)_8{\cdot}4H_2O]_\infty$	50	50	54(1)	46(1)
$[Tb_{0.8}Eu_{1.2}(mip)_3(H_2O)_8{\cdot}4H_2O]_\infty$	60	40	64(1)	36(1)
$[Tb_{0.6}Eu_{1.4}(mip)_3(H_2O)_8{\cdot}4H_2O]_\infty$	70	30	74(1)	26(1)
$[Tb_{0.4}Eu_{1.6}(mip)_3(H_2O)_8{\cdot}4H_2O]_\infty$	80	20	82(1)	18(1)
$[Tb_{0.2}Eu_{1.8}(mip)_3(H_2O)_8{\cdot}4H_2O]_\infty$	90	10	91(1)	9(1)